

Gas and Dust Emission from the Nuclear Region of the Circinus Galaxy

Marcella Contini¹, M. Almudena Prieto^{2,3} and Sueli M. Viegas⁴

¹ School of Physics and Astronomy, Tel-Aviv University, Ramat-Aviv, Tel-Aviv, 69978, Israel

² Max-Planck-Institut für extraterrestrische Physik, D-85748 Garching, Germany

³ Instituto Astrofísica de Canarias, E38200 La Laguna, Tenerife, Canary Islands, Spain

⁴ Instituto Astronômico e Geofísico, USP, Av. Miguel Stefano 4200, 04301 - São Paulo, SP, Brazil

Running title : Gas and Dust Emission from Circinus

Key words : galaxies : Seyfert ; galaxies : individual : Circinus - Line: formation - Continuum: emission

Proofs to be sent to M. Contini (contini@ccsg.tau.ac.il)

Abstract

Simultaneous modeling of the line and continuum emission from the nuclear region of the Circinus galaxy is presented. Composite models which include the combined effect of shocks and photoionization from the active center and from the circumnuclear star forming region are considered. The effects of dust reradiation, bremsstrahlung from the gas and synchrotron radiation are treated consistently. Models which fit the continuum energy distribution of Circinus are used to constrain all possible models suitable for the line emission; altogether are aimed to converge to a most probable representation of the central emission region of Circinus.

The proposed model accounts for two important observational features. First, the high obscuration of Circinus central source is produced by high velocity and dense clouds with characteristic dust-to-gas ratios above 10^{-12} . Their large velocities, up to 1500 km s^{-1} , place them very close to the active center. Second, the derived size of the line emitting region ($\sim 13 \text{ pc}$) is well in agreement with the observed limits for the coronal ($< 10 \text{ pc}$) and narrow line region ($\sim 30 \text{ pc}$) of Circinus.

1 Introduction

Multiwavelength continuum and line data information for a key number of active galactic nuclei (AGN) in the closer Universe is rapidly growing up and becoming more and more complete. The availability of such multiwavelength dataset allows a more detailed and consistent study of the nuclear emitting regions and is definitively demanding more elaborated spectral modeling approaches.

The Circinus galaxy (A1409-65) was first reported by Freeman et al. (1977) with coordinates (1950) R.A. $14^{\text{h}}09^{\text{m}}17^{\text{s}}.5$, Dec. $-65^{\circ}06'19''$; $l=311^{\circ}.3$, $b=-3^{\circ}.8$. Because of its proximity (at a distance of about 4 Mpc), the Circinus galaxy shows one of the richest optical - IR nebular spectrum among AGN. The large range of ionization levels and line strengths immediately suggests the presence of a variety of clouds in the nuclear region having different physical conditions and excited by different mechanisms.

Circinus shows a spectacular, one side [OIII] 5007 ionization cone with apex at the nucleus of the galaxy (Marconi et al. 1994). This asymmetry is probably due to extinction by the galaxy disk which is inclined by about 65 degrees, hiding the counter ionization cone to the observer. Circinus also shows a prominent dust lane South-West of its nucleus (Marconi et al.) which might be causing the obscuration of the intrinsic nuclear light, in particular considering the non detection of Circinus nucleus in the UV light.

In most known Seyfert galaxies residing in spirals, the AGN light is contaminated by circumnuclear star forming regions which largely complicates the interpretation of the line and continuum spectra from the active nucleus. Circinus is not an exception: its Seyfert 2 nucleus resides on a Sb-d system and several pieces of evidence indicate outgoing star formation in the nuclear vicinity. Resolved star formation is seen up to ~ 10 arcsec from the centre, where a ring shaped region is detected (Marconi et al. 1994), whereas CO band absorptions - most probably from red supergiants - are

seen within the inner 0.75 arcsec region (Maiolino et al. 1998). Thus, lines from low ionization states in the nuclear spectrum might include substantial contribution from the stellar activity. On the other hand, lines from highly ionized species, essentially above ion IV, are expected to be produced by radiation from the active center (AC).

Besides the starburst contribution, the AGN emission can itself be dominated by two competing mechanisms, namely, the ionizing radiation from the AC and the shocks. Line and continuum emissions from Circinus indicate that both mechanisms are active. They also reflect the different physical conditions of the clouds from which they arise, including the effect of dust. Therefore, if a meaningful representation of the nuclear region is sought, any modeling of the continuum and of the line emission should be consistent with each other.

Previous modeling of Circinus by Oliva et al. (1994), Moorwood et al. (1997), and Binette et al. (1997) provides a first notion of the complex structure of Circinus nuclear region. In all of the three cases the analysis and results are exclusively based on the modeling of the high ionization line spectrum. However, the available data from Circinus span from radio to X-ray, which requires a self consistent model to explain the complete dataset. Gas emission accounts for most of the continuum and for the lines from high and low ionization levels, whereas dust emission accounts mostly for the IR continuum. Thus, the emission from gas and dust should be calculated consistently, and their effects properly weighted in the different regions of the electromagnetic spectrum. In the modeling of Circinus, several models are used: some provide a better fit to the line spectrum, whereas, others fit better the continuum.

Modeling is based on hypothesis about the symmetry of the region, stellar emission, central source energetics, etc., which added to the input parameters (velocity field, density, dust characteristics) lead to a description

of the real galaxy complex. It is difficult to establish errors of the theoretical results since they depend on atomic and molecular data, some of them being still roughly estimated. Therefore, the most probable model should be selected among the best fitting to the observational data throughout consistency.

This paper is devoted to a self consistent treatment of the continuum and narrow emission line spectra from an AGN. A multiwavelength modeling of the nuclear and extended emission region in the Seyfert 2 NGC 5252 was presented in a similar way (Contini, Prieto & Viegas, 1998). The modeling approach is based on previous work by Viegas & Contini (1997 review and references therein) which focuses on the coupled effect of photoionization and shocks.

The paper is organized in the following way. In §2 the observational dataset for Circinus is given. The general model and the input parameters are presented in §3. A grid of single-cloud models for the Circinus galaxy and the fit to the observed line spectra by multi-cloud models are discussed in §4. The spectral energy distribution (SED) of the continuum given by these models as well as by other models necessary to explain specific features of the continuum appear in §5. The consistent fit of selected multi-cloud models to the line and continuum spectra are discussed in §6. Conclusions follow in §7.

2 Observational dataset for Circinus

Continuum and line data for Circinus were collected from the literature. The continuum emission is well sampled from the X-ray to radio waves with the exception of the UV region; line emission was collected from the optical to the middle IR. In all cases, data from the smallest available aperture were considered in order to minimize the stellar light contribution. Data sources are listed below.

Circinus was detected in the ROSAT “all sky survey” with a flux of about 10^{-11} erg cm $^{-2}$ s $^{-1}$ in the 0.1-2.4 keV (Brinkmann et al. 1994). The X-ray spectrum of Circinus was obtained by ASCA (Matt et al. 1996). The authors derived a 2-10 keV flux of $\sim 10^{-11}$ erg cm $^{-2}$ s $^{-1}$, and a spectral index of -0.5 ± 0.5 . Matt et al. argue that above 2-3 keV, the ASCA emission is mainly reflected X-ray radiation, at the level of a few percent, from an otherwise invisible nucleus even at 10 keV. Moorwood et al. (1997) suggest that the intrinsic ionizing spectrum has the same power-law as the reflected one, and that the observed X-ray emission at 10 keV is about 1% of the intrinsic AGN luminosity at that frequency. We thus adopt the intrinsic nuclear emission radiation at 10 keV to be $\sim 2 \times 10^{-9}$ erg cm $^{-2}$ s $^{-1}$ as in Moorwood et al. (1997).

The optical continuum and line spectra are taken from Oliva et al. (1994). These data cover the 4000-10000 Å region and are integrated over the central 1.5x4.5 arcsec region.

The near-IR line spectrum between 1 and 4 μ m is also taken from Oliva et al. These data are integrated within a rather large aperture, 4.4x6.6 arcsec, and so, only the coronal line fluxes are used for the modeling purposes. The data were cross-checked with much higher spatial resolution data collected in the K band by Maiolino et al. (1998). In this case, the K nuclear emission lines were integrated within a 0.75 arcsec aperture. The coronal line in common to the two dataset, [SiIV] 1.96 μ m, measures $\sim 15\%$ less in the 0.75 arcsec aperture, which is consistent within the errors with a point like origin for the coronal lines.

Middle IR line data between 3 and 40 μ m are provided by ISO (Moorwood et al. 1997). ISO apertures are large, above 20 arcsec, and so, emission from the circumnuclear star-forming ring is included.

For the IR continuum between 1 and 10 μ m two different sources were used. Moorwood & Glass (1994) data from a 5 arcsec aperture were com-

plemented with those from Siebenmorgen et al. (1997) collected in a much smaller aperture typically 0.3 arcsec at 3.8 and 4.8 μm and 1.3 arcsec at 10.3 μm . The datasets are in remarkably agreement. Different aperture photometry at 13 μm by Moorwood & Glass also indicates the point-like nature of the emission. Thus, for the modeling purposes it can be safely assumed that the *IR continuum emission at least in the 3 to 15 μm region originates very close to the AC and is not polluted by circumnuclear star formation activity.*

Below 2.2 μm , the stellar contribution in Circinus is very significant. Maiolino et al. (1998) provide a stellar-corrected flux at 2.2 μm derived from a 0.15 arcsec aperture which turns to be an order of magnitude lower than the integrated value by Moorwood & Glass (1994) in the 5 arcsec aperture. Both set of values shall be considered in the modeling as reference limits to the stellar and pure AGN contribution.

The far IR continuum data above 15 μm were collected from large apertures. Data points at 25 μm (14x20"), 30 and 40 μm (both from 20x30") were directly measured from the ISO 2-40 μm spectrum. The IRAS flux at 25 μm agrees within 18%.

Data at 60, 100 and 150 μm were taken from the spatial resolution analysis by Ghosh et al. (1992), and correspond to an aperture of about 40 arcsec, which is the deconvolved size of Circinus at $\lambda > 50 \mu\text{m}$. Circinus was not detected at 150 μm and so we used the 5 sigma upper limit suggested by Ghosh et al.

Radio data at 5, 2.7 and 1.4 GHz were taken from the Parkes catalogue (Wright & Otrupcek 1990). The data point at 4.85 GHz was taken from Wright et al. (1994), and corresponds to a beam size of 5x5 arcsec and agrees with the 5 GHz Parkes data within less than 1%. Radio emission at 408 MHz was taken from Large et al. (1981) and corresponds to a circular beam size of 43 arcsec.

The nebular spectrum was corrected for internal extinction by $A_V \sim 5$ mag as determined from the H recombination lines. The continuum data were corrected for interstellar extinction in the direction of Circinus by $A_V \sim 1.5$ mag.

The nuclear line profiles in the optical and IR are so far unresolved at the limit of the available observations. FWHM of less than $\sim 150 \text{ km s}^{-1}$ are derived from Oliva et al. (1994) for the optical and near-IR coronal lines and in the range $150\text{-}300 \text{ km s}^{-1}$ from Moorwood et al. (1997) for the ISO lines. Prominent blue wings are seen in the high excitation lines from the nucleus and within the ionization bicone (Vielleux & Bland-Hawtorn 1997) suggestive of outflowing gas motions.

3 The general model

A description of the methodology and application of the modeling approach can be found in Contini et al. (1998) and a more extended discussion in Viegas & Contini (1994, 1997). A model for the narrow-line region (NLR) is proposed. In the model, the circumnuclear clouds move radially outward from the AC and a shock-front is formed on the outer edge of the clouds. The photon flux from the active source reaches the clouds on the inner edge opposite the shock front. Black body radiation from the stars reaches either the inner or the outer edge of the clouds depending on location of the stars.

The SUMA code (Viegas & Contini 1994) is adapted to calculate the emission spectra (lines and continuum) from a shocked cloud which may also be photoionized by a power-law radiation from the central source and a black body stellar radiation. The code consistently calculates shock and radiation effects in a plane-parallel geometry. The calculation of dust reradiation is also included.

The input parameters to the models are the shock velocity, V_s , the preshock density, n_0 , the magnetic field, B_0 , the ionizing radiation flux from the AC which is characterized by the flux at the Lyman limit F_H (in number of photons $\text{cm}^{-2} \text{s}^{-1} \text{eV}^{-1}$) and the spectral index, α . Black body radiation from the starburst is characterized by the temperature of the stars, T_* , and the ionization parameter, U . The amount of dust is given by d/g , the dust-to-gas number ratio. D is the geometrical thickness of the clouds. Cosmic gas abundances from Allen (1973) are used. The values of F_H and V_s determine the type of prevailing model, i.e., radiation dominated or shock dominated.

3.1 Observational constraints to the input parameters

A grid of models characterized by different values of the input parameters is calculated for Circinus. The ranges of the input parameters are selected to match the observed values as follows :

- The intensity of the radiation flux, F_H (in number $\text{cm}^{-2} \text{s}^{-1} \text{eV}^{-1}$) is in the range $10^9 - 10^{12}$, depending on the distance of the illuminated clouds from the AC. These values are derived from the diagnostic diagrams presented in Viegas-Aldrovandi & Contini (1989) and are consistent with Lyman photon number estimates ($\sim 10^{53.5} \text{s}^{-1}$ derived from Moorwood et al. 1997) if the emitting clouds are at 30 pc to 1 kpc from the nucleus.

- A composite ionizing spectrum with spectral index $\alpha_{UV} = 1$, and $\alpha_X = 0.4$ is assumed for all models. In the UV region, $\alpha_{UV} = 1$ was adopted on the basis of the observed He II 4686 / $H\beta$ ratio. The choice of the X-ray spectral index is based on the ASCA spectrum of Circinus (see §2).

- The shock velocities, V_s , are assumed to be less than or about 100 km s^{-1} , as deduced from the FWHM of the emission line profiles (see §2).

Larger velocities will be further discussed when modeling the SED of Circinus.

- Preshock densities are limited by the observed $[\text{SII}] 6717/6730 \geq 1$. Values between 100 and 300 cm^{-3} are assumed. Models with higher densities shall also be considered and discussed in relation to the continuum emission.

- The geometrical thickness of the clouds within the NLR region, D , is defined by the best fit of the spectrum and ranges between 5×10^{17} and 10^{19} cm. This range of values is consistent with the observed size of the coronal line region, <10 pc (Maiolino et al. 1998; Oliva et al. 1994), and of the NLR, ~ 30 pc (Marconi et al. 1994).

- The range of dust-to-gas ratio, d/g , is taken in the range $10^{-14} \leq d/g \leq 5 \times 10^{-12}$. These values are essentially determined by the shape of the middle and far IR continuum respectively. This will be discussed in §5.

- The magnetic field strength is taken $B_0 = 10^{-4}$ gauss following Contini & Aldrovandi (1986).

4 The line spectrum

On the basis of the above observational constraints a grid of suitable single-cloud models for Circinus is proposed. The input parameters characterizing each model are presented in Table 1. As a first step, we shall focus on the modeling of the line spectrum; the continuum analysis will follow as a second step. Notice, however, that *modeling the line and continuum spectra simultaneously implies cross-checking of one another until a fine tuning of the models is obtained.*

4.1 Grid of single-cloud models

The line ratios calculated for each of the models in Table 1 are presented in Table 2. They are given relative to $H\beta=1$. Table 2 illustrates the trends

in the emission line intensities when modifying the input parameters within a reasonable range of values compatible with the observational constraints (§3.1).

Models RD0 to RD5 are characterized by different values of the radiation flux, density, shock velocity and geometrical thickness of the cloud. The ionizing radiation flux, F_H , is progressively increased from RD0 (pure shock model with $F_H = 0$) to RD5.

Model BD is the only one intrinsically different from the rest of the models presented in Table 1. It represents a cloud with $V_s = 100 \text{ km s}^{-1}$ and $n_0 = 100 \text{ cm}^{-3}$ photoionised by a black body. Models with different values for the T_* and U were calculated. Among those, a model (BD) with $T_* = 7 \times 10^4 \text{ K}$ and $U = 0.01$ was selected as it was found to provide the best fit to the optical- near IR SED (cf Fig. 1a) and, as much as possible, to the line ratios. Maiolino et al. suggest that Circinus could be experiencing an outward propagating starburst with the current activity being occurring mainly at the 200 pc radius starburst ring (Maiolino et al. 1998). Therefore, model BD is calculated assuming that radiation reaches the very shock front edge of the clouds.

Table 1 also includes two shock-dominated models, SD1 and SD2, characterized by both large shock velocities and large densities, and a radiation-dominated model, DD, with high density. They shall be discussed when modeling the continuum SED of Circinus (§5).

The lines in Table 2 are grouped following ionization levels, and line ratios lower than $5 \cdot 10^{-4}$ are omitted. In this way it is easy to realise that a spectrum characterized by both strong low ($\leq \text{II}$) and high ($\geq \text{VII}$) ionization lines cannot be fitted by single models. Table 2 shows that models characterized by a low ionization flux, F_H , contribute mostly to lines in the optical range and to low ionization lines in the IR range. RD0 is a shock dominated model with $F_H = 0$ which contributes mostly to the neutral and low ioniza-

tion lines. RD1, with low V_s and low F_H , shows relatively strong II, III, and IV lines. RD2 has higher V_s , n_0 , and F_H , and a geometrical thickness large enough to provide a transition zone where strong neutral and singly ionized lines are emitted. High ionization models (RD3, RD4, and RD5) contribute to the high ionization lines. RD3 and RD4 show relatively strong [Mg VII] 5.5 and [Mg V] 5.6 lines. RD4 has a lower n_0 than RD3 and a larger D , therefore, the stratification of the ions is different, and the emitted spectrum is different. In particular, $[\text{Fe X}]/[\text{Fe VII}] > 1$ and $[\text{Fe XI}]/[\text{Fe VII}] > 1$ are given by model RD5, which is matter-bound with a high F_H ; this model provides also strong lines from species $\geq \text{IV}$, but, being matter bound, negligible neutral and singly ionized lines.

Besides, the black body model BD produces relatively strong lines of levels II and III but negligible highly ionized ions or singly ionized and neutral species.

The trends shown in Table 2 indicate that within the restricted range of densities and velocities allowed by the observations (§3.1), no single-cloud model can account for the observed high, intermediate and low ionization species simultaneously. The intermediate ionization lines (II, III) may be largely dominated by the contribution from star forming regions. Conversely, the highest ionization lines and, to less extent, the neutral lines should be dominated by AC radiation. Thus, a combination of different ionization and excitation conditions represented by different single-cloud models seems unavoidable.

4.2 Fitting the emission-line spectrum

To account for the different excitation conditions in Circinus, several multi-cloud models are studied. Focusing on the line spectrum, three suitable single-cloud combinations, MA, MB, and MC are proposed. The resulting line spectrum is presented in Tables 3a (ground dataset, ratios relative to

[OIII] 5007) and Table 3b (ISO dataset, ratios relative to [O IV] 25.9 μm). The choice of [OIII] 5007 as a reference line instead of the classical $\text{H}\beta$ is based on two facts: [OIII] 5007 is the strongest line in the optical spectrum and is less polluted by the starburst contribution than $\text{H}\beta$. The same arguments apply for the [O IV] 25.9 μm in the ISO dataset. Note that this line is usually absent in ISO spectra of starburst galaxies.

The estimated errors for the ISO data are about 30%. No errors for Oliva et al's ground dataset are reported and so, we assume 15% error for the strongest lines, and 30% for the weak lines and near-IR lines.

The first two composite models, MA and MB, are based on the best fit of the power-law radiation dominated models RD1 to RD5. A third model, MC, considers the additional effect of a young stellar population represented by model BD. The relative weights (W) of individual models in each composite model are given at the bottom of Table 1. Their contributions (P) normalised to the [OIII] 5007 flux are also given in Table 1.

Power-law radiation dominated models: MA and MB

The main difference between MA and MB lies on the emission contribution from larger clouds (model RD4) included in the MB spectra.

Table 3a shows that the high ionization lines above species IV, including the series of Fe lines, are well reproduced by any of the models, the best match being perhaps obtained by model MA. However, discrepancies at the level of 50% or larger appear for the high ionization Si lines: [SiVI], [SiVII] and [SiIX].

Regarding the ISO lines (Table 3b), large discrepancies are again found for the two available [SiIX] lines at 2.59 and 3.9 μm and for [MgV] 5.6 μm . Notice, however, that both [SiIX]2.59 μm and [MgV] 5.6 μm show very weak in the ISO spectrum and, therefore, their fluxes are very uncertain. Moreover, [SiIX]3.9 μm , the only line in common to both ground and ISO

dataset, is a factor of 2 larger in the ISO dataset. The remaining ISO high ionization lines are reproduced by the models, in particular by model MB, within the 30% observational error.

Intermediate ionization levels (II and III) in the ground dataset are well reproduced by the models, with MA providing in general a better match. The exceptions are [OII] 7320 and [SIII] 9913, overestimated by about 50%. Major discrepancies are found with the intermediate levels in the ISO dataset, which are underestimated by large factors, in particular, the [SIII] 33.5 μm , [NeII] and [SiII] lines. On the other hand, [FeII] 26 μm is overpredicted by factors between 2 and 3.

Ground based neutral lines in Table 3a are underestimated by factors between 2 to 3 with the marginal exception of [CI] 9850. This result is not improved if the shock dominated model, RD0, which presents the strongest neutral lines, is included.

The systematic differences found for the lines from lower ionization ions can be understood in view of the starburst contribution in Circinus. This becomes indeed more important for the ISO lines due to the larger aperture used, definitively including Circinus star-forming ring.

Power-law + black-body radiation-dominated model: MC

The contribution from the young stellar population to the central emission is considered in model MC, which includes the results of the hot black-body model BD. Because the ISO apertures are much larger than those used for the ground data, model MC attempts to account for the ground-base dataset while keeping reasonable agreement with ISO high ionization species.

Our calculations show that only black-body contributions (relative to [OIII] 5007 flux) larger than 30% leads to sensible differences between MC and models MA, MB. The exact contribution of model BD to MC is pre-

sented in Table 1, and it is derived from the fit of the continuum in the optical range (Fig. 1a). Clouds ionized by a low ionization power-law flux (models RD1-RD2) contribute as much as 36 % to the [OIII] 5007 line flux, whereas, those ionized by a stronger flux (RD4-RD5) contribute about 30%. Low ionized clouds could be interpreted as regions being at larger distances from the nucleus and/or with low covering factors. Their larger contribution is explained by a large number of clouds. Notice that their geometrical thickness is small.

The resulting line spectrum is presented in Tables 3a and 3b. A slight overall improvement over the previous models is achieved, though larger discrepancies still hold for the relatively weak lines [NI] 5200 and [OII] 7320. High ionization lines are also sensitive to this model and, thus, improved fits for [Si IX] 3.9 μm and marginally for [SiIX] 3.9 μm are obtained (Table 3a). However, this is not the case for the ISO lines [Mg VIII] 5.5 μm and [Ne VI] 7.6 μm , which worsen by 50%. As expected, ISO low ionization species remain largely underpredicted.

Let us recall that, although the best fit to the line spectra was searched throughout a wide range of the input parameters, these were restricted by the observational data as described in §3.

4.3 Relative abundances

The models in Table 1 are all run with cosmic abundances from Allen (1973), with the exception of S/H which is lower by a factor of 1.4. These assumptions are based on previous modeling of AGN (e.g., Contini et al. 1998). Ferguson et al. (1997) propose a different set of relative abundances. One of the main differences is the S/H value, which these authors increase by 60% relative to the cosmic values. Larger S/H should give a better fit to the IR lines but worsens the fit to the optical [S II] 6717,6731 lines. On the other

hand, Ferguson et al's values for He/H, Ar/H and Mg/H are expected to lead to an improvement of the current line fit.

Grains are nearly unspattered downstream for models RD0-RD5 because of their relatively low shock velocities. Therefore, low S/H values would also imply low Si/H, O/H, and Mg/H. A lower Si/H would improve the fit of [Si IX] lines if oxygen were less depleted than Si.

If the line ratios are considered as Abundance Ratios Indicators (cf. Table 2 from Ferguson et al. 1997), our results give $[\text{Mg VII}]/[\text{Si VII}] = 2.37$ and $[\text{Mg VIII}]/[\text{S IX}] = 2.5$, well included between the lower and upper values of Ferguson et al. (1997), 1.3-2.5 and 1.8-3.0, respectively.

5 Continuum radiation

Modeling the continuum energy distribution is not always as straightforward as it is for the line spectrum. Bremsstrahlung from very dense gas is absorbed in the radio-far IR (FIR) range. FIR and middle IR emissions are produced by dust grains at different temperatures. In the near IR-optical range black body radiation from old stars in the galaxy prevails in some galaxies. Correction for stellar emission is a delicate issue and can mislead the data. In the hard X-ray domain the flux from the AC is directly observed, while bremsstrahlung from heated gas is seen in the UV and soft X-ray ranges.

Gas at very high ($> 10^5$ K) and very low temperatures ($< 10^4$ K) is clearly recognized in the SED of the continuum. Particularly, high temperatures are responsible for soft X-ray emission and for grain reradiation in the mid IR. Low temperature gas refers to the radio range where bremsstrahlung and synchrotron radiations are of competing strengths.

Therefore, models which explain the line spectra are not always sufficient to fit the entire SED of the continuum.

In modeling the line spectrum of Circinus it was found that clouds reached by different flux intensities and covering a narrow range of densities and velocities can account for the observations. To further investigate the validity of the proposed models, these are checked against Circinus multifrequency continuum data. Though models MA, MB, and MC give a reasonably approximation to the overall line spectrum, we shall show in the next sections that none of them can fully account for the overall radio-to-X-ray continuum trend and that some additional conditions outside the range covered by the line-fitting models are required. On the basis of the continuum data, three new additional models are proposed : two shock-dominated models (SD1 and SD2), characterised by high shock-velocities and densities, and a radiation-dominated high-density model (DD).

The analysis of the continuum emission will follow procedures similar to those used for the line ratios. After the analysis of the continuum emission components in Circinus (§5.1), a series of single-cloud models are discussed: those suggested by the fit to the line spectra are verified for the SED in §5.2. Additional models required to explain some features of the continuum are presented in §§5.3 and 5.4.

Dust emission has an important role in modeling the IR continuum when shocks are present as it depends on the energy gains of the grains by collision and by radiation. A comparison between these two processes is presented in Appendix 1 for the most significant single-cloud models. Finally, synchrotron emission by Fermi mechanism (Bell 1978) can be generated via shocks. This is the case of the radio emission in supernova remnants where shocks are the main source of heating and ionization of the gas. Details on the synchrotron emission in Circinus are presented in Appendix 2.

5.1 Continuum emission components in Circinus

The available data for the SED of Circinus continuum are shown in Fig. 1a. Depending on the spectral range, different emission components contribute to the observed continuum with different importance.

First of all, the emission from the underlying old stellar population associated with Circinus host galaxy contributes mainly in the optical domain. A black body spectrum with $T = 2000$ K (model BB hereafter) is found to provide a reasonably fit to the observed SED in the 0.4 to $2 \mu\text{m}$ range (dash-dotted line in Fig. 1a). From hereafter, in all proposed models this component shall be fixed and normalised to the observed emission at about $2 \mu\text{m}$. The derived stellar-subtracted emission at $2 \mu\text{m}$ by Maiolino et al. (1998) is represented by an asterisk in Fig. 1a. We will use this value as a reference for the non-stellar contribution to the continuum emission.

Following Matt et al. (1996) arguments, the intrinsic X-ray AGN continuum source is assumed to be totally absorbed below 10 keV. In Fig 1a, the cross in the X-ray domain represents the intrinsic 10 keV flux derived under the assumption that the observed ASCA flux at 10 keV is 1% percent of the intrinsic AGN flux. The dotted line is the absorbed ionizing continuum.

In the current modeling any UV to soft X-ray emission is assumed to be due to bremsstrahlung from shock-heated gas. The strong obscuration towards Circinus nucleus prevents the detection of Circinus in the UV, but ROSAT observations provide a $0.1 - 2.4$ keV integrated flux. This information shall be used to constrain the bremsstrahlung component, and will be discussed in connection with the shock-dominated models (§5.4).

The second important bremsstrahlung component is due to gas heated by radiation (AGN and starburst) to temperatures of about 10^4 K. This component extends its contribution from the optical - where it peaks - to the radio domain.

The mid and far IR continuum radiation is assumed to be due to re-

radiation by dust at different temperatures. Dust is heated by both radiation and shocks. The modeling of the mid-to-far IR SED essentially determines the dust-to-gas ratio parameter, d/g , which in turn is used as an input value for the modeling of the line spectrum. Notice that in the process of fitting the various continuum emission components, and, in the end, the continuum and line spectra together, an overall consistency is sought. In particular, the bremsstrahlung emission components should be consistent with the position of the IR bumps (cf Appendix 1) since the temperature of the dust grains follows the temperature of the gas (Viegas & Contini 1994).

Radio emission is coming from synchrotron and bremsstrahlung processes. We shall see that synchrotron emission (cf Appendix 2) appears to be the dominant component.

5.2 The SED of radiation dominated single-cloud models

The SED associated with each of the models RD1 to RD5 (labeled 1,2,3,4,5) and BD are shown in Fig. 1a. Their relative contributions is defined by their weights (cf. W in Table 1), and so they are shifted in the figure according to the W values, with RD2 bremsstrahlung component being normalised to the observed optical continuum emission at $6.16 \cdot 10^{14}$ Hz. In doing so, it is implicitly assumed that the bremsstrahlung component is much weaker than the emission contribution from Circinus underlying stellar population (model BB, dash-dotted line). An alternative normalization may have been Maiolino et al's stellar-subtracted continuum emission at $2\mu\text{m}$ (marked with an asterisk in Fig 1a). However, this option was dropped because it leads to an overestimation of the predicted emission compared to the observed values at wavelengths shorter than $2 \mu\text{m}$.

Having settled the model normalization, the resulting scenario is as follows. The direct AGN flux seen through the clouds is mainly accounted for

by model RD2 (dotted curve in the high frequency range). The predicted flux at 10 KeV can be reconciled with the ASCA flux if this is taken to be $\sim 2\%$ of the intrinsic emission, in agreement with the AGN reflection estimate by Matt et al. (§2). The contribution of the other RD models is negligible and is not represented in the figure. For example, model RD1 that has the highest weight, yields a negligible contribution to the hard X-ray due to its low F_{H} value (Table 1). Also negligible is the contribution of the high ionization model RD5 because of its low weight.

Model BD, representing the starburst contribution, is also plotted in Fig. 1a and shifted according to its weight (Table 1) in the multi-component model MC. As mentioned above, BD was selected among several black body radiation dominated models because of best fitting the SED of the continuum in the optical range.

Due to the high extinction in Circinus, no UV data of the galaxy are available. We thus assume that the starburst ionizing continuum represented by a $T_{*} = 7 \cdot 10^4$ K black-body is fully absorbed.

The dust emission component associated with RD and BD models peaks in the far-IR region (Fig. 1a). The maximum temperature of the grains is about 30 K for model RD1, and 50 K for model RD2 (cf Figs. 3a and 3b). The continuum emission beyond $2 \cdot 10^{12}$ Hz readily constrains the dust-to-gas ratio to $d/g < 10^{-14}$. Note that due to its larger weight, the contribution of model BD to the optical and near-IR is more important than that due to the RD models.

In the radio domain the main contribution to the emission is due to synchrotron radiation calculated by models BD and RD4 (straight lines in Fig. 1a). The other models give a negligible contribution and are not represented. The corresponding bremsstrahlung components associated with models BD and RD are far less important and furthermore show different trends than observed (Fig. 1a).

5.3 High density clumps : model DD

The sharp cut-off observed in the SED at $2 \cdot 10^{12}$ Hz strongly constrains the d/g parameter. Absorption by high density matter may be causing the fall of the emission at this low frequencies. Following Kirchoff's law, the absorption coefficient, κ , can be expressed as:

$$\tau_\nu = \int \kappa ds = 8.24 \cdot 10^{-2} T^{-1.35} \nu^{-2.1} E \quad (1)$$

with T, the temperature, in K, ν in GHz and $E = \int n_+ n_e ds$ in $\text{cm}^{-6} \text{ pc}$ (Osterbrock 1989). Adopting $T = 10^4$ K, $ds = 100$ pc and $\nu = 2 \cdot 10^3$ GHz, values of $\tau_\nu > 1$ are obtained for densities $n > 5 \cdot 10^5 \text{ cm}^{-3}$.

Such high densities could result from compression downstream of shocked gas with densities $n_0 \geq 5000 \text{ cm}^{-3}$. This section investigates the role of a model, DD, characterized by $n_0 = 5000 \text{ cm}^{-3}$. DD is a radiation-dominated model also characterised by cloud velocities $V_s = 250 \text{ km s}^{-1}$ and Lyman flux $F_H = 10^{12}$ (Table 1). In the downstream region the densities rise to $\sim 5 \cdot 10^5 \text{ cm}^{-3}$, and radiation is absorbed for $\nu \leq 2 \cdot 10^{12}$ Hz.

Fig 1b shows the SED associated with model DD (solid line). The normalization of this model is such that it matches the observed far-IR peak emission. In doing so, the dust-to-gas ratio is settled to $d/g = 4 \times 10^{-12}$. Radiation is absorbed for $\nu \leq 2 \cdot 10^{12}$ Hz and, indeed, the model prediction below this frequency (dotted line) should be taken as an upper limit. In addition, the synchrotron component associated with model DD provides a satisfactory fit to the observed radio emission. The high absorption does not apply to the synchrotron component which is created at the very shock-front edge of the clouds.

The line spectrum from model DD is included in Table 2. Notice that due to the high density adopted, the lines with low critical density for collisional de-excitation ([NI], [SII], etc) are very weak, and all species above level IV

are negligible due to the mutual effects of high F_H , high V_s , high n_0 , and a small D on the stratification of the different ions downstream. Model DD can account for the far-IR and radio SED, but the mid-IR SED is still not reproduced. Furthermore, DD bremsstrahlung component is overpredicting the stellar-subtracted emission at $2 \mu\text{m}$ (asterisk in Fig. 1 b). To fill up the middle IR region, hotter dust is required. Higher temperatures of both gas and dust can be reached via stronger shocks. Therefore, shock-dominated models are introduced in the SED modeling (next section).

5.4 Shock-dominated spectra from high velocity clouds: models SD1, SD2

In previous sections we have modeled the line spectra and part of the SED of the continuum. Still the data in the soft X-ray range and in the middle IR are unfit. We recall that the temperature of the grains follows the temperature of the gas, therefore, models characterized by higher temperature should be included in the final average. This section analyses the impact of shock-dominated high velocity models on the overall spectrum.

Two shock-dominated models, SD1 and SD2, are proposed. Model SD1 is characterised by a cloud velocity $V_s = 400 \text{ km s}^{-1}$ and a density $n_0 = 300 \text{ cm}^{-3}$, and model SD2 by $V_s = 1500 \text{ km s}^{-1}$ and $n_0 = 1000 \text{ cm}^{-3}$. The SED generated by these models are represented by dashed lines in Fig. 1b. The respective bremsstrahlung components calculated with these models peak in the soft X-rays. These models are normalised as to account for the observed 0.2-2.4 keV integrated flux, $F_X = 1.3 \cdot 10^{-11} \text{ erg cm}^{-2} \text{ s}^{-1}$ (cf §2), and the mid-IR continuum emission. These in turn impose $d/g \sim 5 \cdot 10^{-12}$.

Regarding dust emission, the adopted value of $V_s = 1500 \text{ km s}^{-1}$ is a lower limit to shock velocities which could be deduced from the location of the IR bump. Indeed, due to sputtering the grains entering the shock front are rapidly destroyed and have no time to cool. However, they survive long

enough because their lifetime is $\tau = 3 \cdot 10^{12} \text{ a}/n \sim 10^4$ years (cf Osterbrock 1989), where a is the grain radius ($\leq 0.2 \mu\text{m}$) and n the gas density ($3000\text{-}5000 \text{ cm}^{-3}$). Such life times in the present conditions correspond to a maximum distance from the shock-front of $\sim 3 \cdot 10^{18} \text{ cm}$, which is reduced by sputtering. In AGN, large velocities generally correspond to large densities, and in turn, to large compression downstream, so, the sputtering of grains entering the shock front will be more effective for large V_s and the grains will be completely destroyed.

The line ratios calculated by models SD1 and SD2 are presented in Table 2. Model SD1 is characterised by weak line fluxes (notice that $\text{H}\beta = 5.5 \cdot 10^{-4} \text{ erg cm}^{-2} \text{ s}^{-1}$), as compared with the radiation-dominated models. Downstream compression is strong for model SD2. The high density and high d/g ratio cause rapid cooling in the emitting line region (dominated by $T_e \sim 10^4 - 10^5 \text{ K}$). Therefore, compared with radiation-dominated models, SD2 line spectrum is relatively weak for species below level IV but strong for levels above.

6 Line and continuum spectra from multi-cloud models

We emphasize that the single models represent prototype clouds in the different regions of the galaxy. The multi-cloud models imply the relative importance (and position) of the single cases and give a more realistic picture of the AGN.

The continuum SED provided by the models which fit the emission line ratios in previous sections could not explain all the features of the observed SED. Two additional types of single-cloud models (shock dominated clouds represented by models SD1, SD2, and the dense clumps represented by

model DD) should be added to the multi-cloud models defined in §4 (MA, MB, and MC).

In the following, the new version of models MA and MC (including the SD clouds) are discussed and referred to as MA+ and MC+. Model MB is very similar to MA and is omitted from the discussion. The weights of the SD models in the composite models MA+ and MC+ (in parenthesis in Table 1), are relatively low, thus preventing any sensitive contribution to the line spectra. Despite the high velocities, 1500 km s^{-1} , implied by the SD2 model, any expected broadening in the emission lines would escape detection due to its relative low contribution to the optical and IR line spectrum. The contribution of SD models is, however, dominant in the soft X-ray domain, and is sufficient to account for the observed integrated flux in the 0.2-2.4 keV. The resulting spectra are shown in Figs 2a and 2b.

Both MA+ and MC+ still fail to reproduce the overall SED of the continuum, even if the weights of the single-cloud models are substantially changed. A further possibility is to include the contribution of the high density radiation dominated model DD which was found to provide an improved fit to the low frequency continuum beyond $2 \times 10^{12} \text{ Hz}$. This corresponds to the multi-cloud model MD.

The relative contribution of the different components to MD is given in Table 1. The main differences from model MC are the increase of the contribution of model BD from 31 % to 47 %, the corresponding decrease of the radiation dominated models (RD) by about the same amount, and the relative minor contribution of model DD. As expected, MD provides a substantial improvement to the fit of the SED over the entire energy range (Fig. 2c), and, relative to the emission line spectra (Tables 3a and 3b), two main differences with respect to model MC arise. Due to the decreased contribution of the radiation-dominated models, most of the high ionization line ratios in MD suffer a slight decrease. Conversely, low ionization line ratios

get substantially increased due to the contribution from high density clouds. Besides, MD line spectrum encounters the same fitting problems already discussed for model MC which essentially relate to the aperture-dependent contribution of the star forming region. Summarizing, optical intermediate ionization levels are reproduced within the observational errors, whereas neutral and low ionization lines remain a source of large discrepancies. In the IR, high ionization levels are reproduced within 30 % to 80 % ; low and intermediate ionization lines are largely underpredicted. Notice, however, the strong improvement in the [NeII] 12.8 / [OIV] 25.9 line ratio.

We recall that model DD, characterized by $V_s = 250 \text{ km s}^{-1}$, implies line profiles with FWHM larger than those predicted by radiation dominated RD models. Considering that model DD only affects the low ionization levels lines (see Table 2), profiles of low ionization lines slightly broader than those from high ionization lines are predicted.

7 The final scenario

The analysis of the multiwavelength line and continuum emission from Circinus has shown that clouds under very different physical conditions contribute to the line and continuum emission. Various models are proposed that provide a fair account of the observed line spectrum, however, the multi-cloud model MD is perhaps the only one providing the closest representation of the continuum and line spectrum simultaneously. Translating the results from that model into physical terms, the proposed scenario for Circinus would be as follows.

Within Circinus central 5 arcsecs, the integrated emission includes the contribution from the AC, a young stellar population and the underlying host galaxy population. The emission from the galaxy central region is a combination of radiation-dominated clouds ionised by the central source and by the starburst, and of shock-dominated clouds with velocities up to

1500 km s⁻¹. Radiation dominated clouds contribute to the optical-IR line spectrum within about 53% (power-law radiation from the AC) and within 47 % (black body radiation from the stars) to the observed [OIII] 5007 emission, whereas, shock-dominated clouds account for the observed soft X-ray and the mid-IR continuum emission.

Radiation dominated clouds are characterised by velocities within the 60 - 100 km s⁻¹ range, densities between 100 and 200 cm⁻³, and dust-to-gas ratios, d/g, less than 10⁻¹⁴, all these parameters being consistent with the observations (§2). The radiation-dominated clouds correspond to a wide range of nuclear ionization fluxes which can be interpreted in terms of a wide range of cloud distances to the AC and cloud covering factors.

In addition to those low density clouds, a small fraction of radiation dominated clouds are characterised by very high densities, $n_0 \sim 5000 \text{ cm}^{-3}$, and $d/g \sim 4 \cdot 10^{-12}$. The contribution of these clouds to the line spectrum is very small; yet, they dominate the low-frequency end of the mid-IR continuum emission and the far-IR emission.

Shock dominated clouds are characterised by velocities up to 1500 km s⁻¹, densities up to 1000 cm⁻³, and are highly dusty with $d/g > 10^{-12}$. Their large velocities place them close to the AC; their large d/g ratios make them consistent with the obscuration of the central source. The contribution of these shock-dominated clouds to the line spectrum is negligible, but they fully account for the observed soft X-ray and mid-IR continuum emission.

The radio continuum in Circinus is mainly synchrotron emission due to Fermi mechanism acting in the shock front edge of the clouds. The total bremsstrahlung component due to the shock-dominated and radiation-dominated clouds is insufficient to account for the observed trend and intensity in the radio waves. The high density clumps provide the strongest contribution to the synchrotron emission.

Finally, a rough estimate of the average distance of the emitting clouds

from the AC can be derived by comparing the observed [OIII] flux ($1.95 \times 10^{-11} \text{ erg cm}^{-2} \text{ s}^{-1}$ at earth, Oliva et al. 1994) with that derived from model MD at the nebula ($13.4 \text{ erg cm}^{-2} \text{ s}^{-1}$). As the larger contribution to the [OIII] flux arises from the highest ionization models, RD4 and RD5 - as it can be easily deduced from Table 1- the distance thus derived will be essentially that of the coronal line region. Assuming a filling factor, f , and a distance of Circinus of 4 Mpc, the comparison of the two values yields $d(\text{pc}) = 4.9 \times f^{-0.5}$. Assuming an average $f = 0.1$, gives $d \sim 13 \text{ pc}$, in reasonable agreement with the observed estimate for the coronal ($<10 \text{ pc}$) and NLR ($\sim 30 \text{ pc}$) sizes.

Acknowledgments

We are grateful to H. Netzer for interesting comments, and to an anonymous referee for constructive criticism. M.Contini thanks the IAG-USP for warm hospitality. This paper is partially supported by FAPESP, CNPq, and PRONEX/FINEP.

Appendix 1 : The heating of dust grains

We have shown in previous sections that the SED of the continuum in the IR range is determined by the temperature of the grains. In this section, dust heating mechanisms are discussed and the distribution of dust temperature throughout the clouds is presented for the most significative models presented in Table 1.

The grains are heated by both radiation from the active center (AC) and collisions (cf. Viegas & Contini 1994) and reradiate in the near IR - IR range. The dust temperature is determined by balancing energy gains and losses.

The energy gain (in erg s^{-1}) for radiation, HF (dot-dashed line), and for collision, HC (solid lines) are compared throughout the cloud in Figs. 3a, 3b, 3c, and 3d (bottom diagrams). In order to better understand the results, the distribution of the gas temperature (solid lines) and of the dust temperature (dashed lines) are shown in top of the figures. Figs 3a, 3b, and 3c illustrate the results of models RD1, RD2, and DD, respectively. Each cloud is divided in two halves. The x-axis scale is logarithmic and asymmetric in order to have a comparable view of the two parts of the cloud. The shock front is on the left while the edge photoionized by the radiation flux from the AC is on the right.

The dust temperature is higher in the immediate postshock region rather than in the photoionized edge, even for a relatively weak shock as for model RD1 (Fig. 3 a). Dust grains are collisionally heated as they pass through the shock front. Therefore, the location of the dust emission peaks in the SED of the continuum (cf. Figs. 1 a and b) are determined by the temperature of the gas in the postshock region, and consequently depends on V_s .

The dust and gas temperatures drop faster downstream for model DD (Fig. 3c) because the density of the gas is high. The temperatures reached in model DD are higher than in model RD2 (Fig. 3b) because V_s is higher,

so the SED peaks at a higher frequency. Notice that for model DD collision heating of the grains always prevails.

Finally, the results of model BD are plotted in Fig. 3d. Radiation heating of the grains prevails through most of the cloud, but collision heating prevails in the region of gas at $T_e \sim 10^4 - 10^5$ K. We recall that in this case radiation reaches the very shock front edge.

The other models of Table 2 are more predictable. For models RD3, RD4, and RD5 radiation heating prevails. However, the temperature of the grains is not higher than that calculated for models which show the same V_s . Therefore, reradiation peaks in the FIR. Regarding shock dominated models (SD1 and SD2) collision heating prevails. Particularly, for SD2, the grain temperature reaches a maximum value of 275 K downstream and the grains survive up to a distance from the shock front of 10^{15} cm. Therefore, reradiation peaks at about $9 \mu\text{m}$.

In conclusion, the presence of shocks is important in the heating of gas and dust to high temperatures. Radiation heating and collision heating are both effective, but collision heating of the grains prevails in the hot region, therefore, the location of the peak corresponding to reradiation by dust in the SED of the continuum depends strongly on the shock velocity.

Notice that in all the models an initial grain size $a = 0.2 \mu\text{m}$ is assumed. A different size could change the temperature results, but not the main conclusions.

Appendix 2 : Synchrotron radiation

Radio emission in Circinus clearly departs from the calculated bremsstrahlung trend (see Figs. 1a and 1b) and suggests that synchrotron emission could be the main component. The case of Circinus is in marked contrast with that of the Seyfert 2 galaxy NGC 5252 for which simple bremsstrahlung could nicely account for the radio SED (cf. Contini et al. 1998, Fig. 1).

Synchrotron radiation due to Fermi mechanism arises from reacceleration of particles through the shock-front, this being located at the outer edge of the cloud facing the observer, while radio and IR bremsstrahlungs are emitted by relative cold gas from the inner region of the cloud and more easily absorbed (cf §5.3). Synchrotron emission is included in the SUMA code, and is consistently calculated with that of the bremsstrahlung. Two power-law spectral index, -0.35 and -0.75, which define the limits between the non-relativistic and the relativistic case respectively, are considered. Among the various models discussed, only the synchrotron radiation associated with model DD provides sufficient emission to account for the observed radio flux (Fig. 1 b), whereas, the other models give negligible contributions. In this case, the -0.75 power-law index reasonably fits the radio trend. If the emission at $2.3 \cdot 10^{11}$ Hz were associated with the synchrotron component, then a much steeper spectral index had to be considered. As shown in Fig 1b, a power-law spectral index of about -0.35 gives a crude approximation to the data.

The cutoff of the synchrotron emission at lower frequencies calculated by model DD must be consistent with the data. Following Ginzburg & Syrovatskii (1965) the presence of a dense plasma reduces and even stops synchrotron radio emission for $\nu \leq 20n_e/B$. As B (downstream) = $B_0 (n_e / n_0)$ the cutoff depends on the preshock magnetic field and on the preshock density. Adopting $B_0 = 10^{-4}$ gauss, the cutoff is at $\nu \sim 10^8$ Hz for low density models, and at $\nu \sim 10^9$ Hz for high density models. The latter is larger than it is observed as emission is still observed up to at least frequencies of $4 \cdot 10^8$ Hz. However, we recall that the magnetic field can be amplified at the shock front by turbulence which is created by collision and fragmentation of high density clumps through R-T and K-H instabilities (Jun & Norman 1995). Consequently, the cutoff could be shifted to lower frequencies.

References

- Bell, A.R. 1978 MNRAS 182, 443
- Binette, L., Wilson, A, Raga, A. & Storchi-Bergmann, T. 1997 A&A 327,909
- Brinkmann, W., Siebert, J. & Boller, Th. 1994, A&A 281, 355
- Contini, M. & Aldrovandi, S.M.V. 1986 A&A 168, 41
- Contini, M. Prieto, M.A. & Viegas, S.M. 1998, ApJ 492, 511
- Ferguson, J.W., Korista, K. T., Ferland, G.J. 1997, ApJS 110, 287
- Freeman et al. 1977, A&A 55, 455
- Ghosh, S.K. et al 1992, ApJ 391, 111
- Ginzburg, V.L. & Syrovatskii, S.I. 1965, Ann. Rev. A. Ap, 3, 297
- Jun, B.-I., & Norman, M.L. 1995 in "Shocks in Astrophysics", eds. T.J. Miller & A.G. Raga (Dordrecht:Kluwer), 267
- Large, M. I., Mills, B. Y., Little, A. G., Crawford, D. F., Sutton, J. M., 1981, MNRAS 194, 693
- Maiolino, R. et al 1998, ApJ 493, 650
- Marconi, A. et al. 1994, The Messenger 78, 20.
- Matt, G. et al. 1996, MNRAS 281, 69
- Moorwood, A.F.M. et al. 1997, A&A 315, L109
- Moorwood, A.F.M. & Glass, I.S. 1984 A&A 135, 281
- Oliva, E. et al. 1994, A&A 288, 457
- Osterbrock, D.E. 1989 "Astrophysics of Gaseous Nebulae, University Science Books, California
- Siebenmorgen R., Moorwood, A., Freudling, W. & Kaufel, U., 1997, A&A 325, 450
- Veilleux, S. & Bland-Hawtorn, J. 1997, ApJ 479, L105
- Viegas-Aldrovandi, S.M. & Contini, M. 1989 ApJ 339, 689
- Viegas, S.M. & Contini, M. 1997, in "Emission Lines in Active Galaxies: New Methods and Techniques". IAU Colloquium N. 159

Viegas, S.M. & Contini, M. 1994, ApJ 428, 113

Wright, A., Griffith, M., Burke, B.F. & Ekers, R.D., 1994, ApJS 91, 111

Wright, A. & Otrupcek 1990, Parkes Catalogue, Australia Telescope National Facility

Figure Captions

Figure 1

a. The comparison of the calculated SED of the continuum with observation data (filled squares). Thin solid lines represent radiation (power-law) dominated models (RD1-RD5) indicated by the relative numbers. Thick solid lines represent the radiation (black body) dominated model BD. The dotted line represents radiation from the AC. The dash-dotted line indicates black body radiation from old stars (see text). The asterisk represents the stellar-subtracted emission at $2 \mu\text{m}$.

b. Same as for Figure 1 a for shock dominated models, SD1 and SD2, (dashed lines) and for model DD (solid lines). At frequencies below $2 \cdot 10^{12}$ Hz the emitted radiation is absorbed and model DD is represented by dotted lines.

Figure 2

The comparison of the calculated SED of the continuum (solid lines) with observation data (filled squares) for the composite models discussed in the text. The dotted line represents the radiation flux from the AC. The dashed lines refer to the absorbed radiation in model DD. The dot-dashed line represents black body radiation from old stars. The asterisk represents the stellar-subtracted emission at $2 \mu\text{m}$.

a. MA+ ; b. MC+ ; c. MD.

Figure 3

a. Top diagram : the temperature of the gas (solid line) and the temperature of dust (dashed line) as function of the distance from the shock front (left) and from the photoionized edge (right) for model RD1. Bottom diagram : the energy gain of grains (in erg s^{-1}) by collision (solid line) and by radiation (dot-dash line).

b. The same as for Figure 3a for model RD2.

c. The same as for Figure 3a for model DD.

d. The same as for Figure 3a for model BD. The shock front and the photoionized edges are on the same side (left).

Table 1
The input parameters of Table 2

	RD0	RD1	RD2	RD3	RD4	RD5	BD	SD1	SD2	DD
$V_s(\text{km s}^{-1})$	60	60	100	100	100	100	100	400	1500	250
$n_0 (\text{cm}^{-3})$	100	100	200	200	160	100	100	300	1000	5000
F	0.	1(9)	1(10)	2(11)	2(11)	4(11)	-	-	-	1(12)
d/g	1(-14)	1(-14)	1(-14)	1(-14)	1(-14)	1(-14)	5(-14)	6(-12)	5(-12)	4(-12)
D (cm)	>4(15)	5(17)	1(18)	6(18)	1.1(19)	9(18)	3.5(17)	2(18)	1(17)	2(18)
$H\beta^*$	2.3(-5)	6.7(-3)	0.05	1.23	1.47	1.6	0.01	5.5(-4)	0.015	2.2(4)
[OIII]*	2.3(-4)	0.08	0.97	23.	47.	67.	0.07	0.016	0.11	11.
W(MA)	-	7.5	1.0	3.6(-3)	-	9.6(-3)	-	(0.16)	(1.6(-3))	-
W(MB)	-	7.4	1.0	3.4(-3)	0.017	8.6(-3)	-	-	-	-
W(MC)	-	7.4	1.0	3.4(-3)	0.017	8.6(-3)	20.	(0.19)	(1.8(-3))	-
W(MD)	-	8.86	1.0	5.(-3)	0.013	0.01	39.7	0.02	4.(-3)	1.6(-4)
P(MA)	-	0.263	0.423	0.036	-	0.279	-	-	-	-
P(MB)	-	0.20	0.32	0.026	0.27	0.19	-	-	-	-
P(MC)	-	0.136	0.221	0.018	0.184	0.131	0.31	(7(-4))	(5(-5))	-
P(MD)	-	0.123	0.168	0.02	0.10	0.12	0.47	5.(-5)	8.(-5)	3.(-4)

* $\text{erg cm}^{-2} \text{s}^{-1}$

Table 2
Calculated spectra ($H\beta = 1$)

	RD0	RD1	RD2	RD3	RD4	RD5	BD	SD1	SD2	DD
[NI] 5200+	0.28	0.025	0.31	-	-	-	0.015	0.03	-	3(-3)
[OI] 6300+	0.53	0.29	3.4	-	-	-	0.10	0.48	0.07	0.15
[CI] 9850	0.74	0.02	8(-3)	-	-	-	0.01	0.27	3(-3)	0.03
[NII] 6548+	12.2	3.75	6.5	0.03	0.01	2.(-3)	2.0	7.6	0.48	0.20
[SII] 6716	3.5	0.94	2.7	-	-	-	0.22	0.34	4(-3)	0.01
[SII] 6730	3.0	0.84	3.4	-	-	-	0.22	0.7	8(-3)	0.03
[OII] 7320+	8.7	0.18	0.3	0.01	-	2(-3)	0.08	10.4	3.0	0.02
[NeII] 12.8	0.3	0.06	0.1	1(-3)	-	-	0.15	0.18	0.02	0.12
Fe II 26	0.32	0.55	1.	-	-	-	0.35	0.05	-	0.05
[SiII] 34.86	1.1	1.62	2.1	-	-	-	1.29	0.033	-	0.02
HeII 4686	7(-4)	0.26	0.32	0.38	0.49	0.66	0.01	0.16	0.39	-
[OIII] 5007+	9.9	12.	19.4	18.8	32.	42.	6.80	28.4	7.7	5(-4)
[SIII] 9069+	4.1	3.3	3.3	0.16	0.04	3(-3)	1.70	1.5	-	0.06
[ArIII] 8.88	0.15	0.4	0.23	0.01	1(-3)	-	0.37	0.1	0.02	0.01
[NeIII] 15.6	0.095	2.	2.7	1.0	0.7	0.18	1.63	0.43	0.04	0.03
[SIII] 18.7	0.37	0.9	0.8	0.03	5(-3)	-	0.60	0.1	3(-3)	6(-3)
[SIII] 33.5	0.56	1.22	1.	-	-	-	0.66	0.026	-	2(-3)
[SIV] 10.54	0.13	0.4	0.13	1.2	0.4	0.02	0.18	0.17	0.01	-
[OIV] 25.9	1(-3)	0.86	1.8	5.2	6.0	4.6	1.4	1.48	0.03	-
[MgV] 5.6	-	2(-3)	6(-4)	0.33	0.33	0.04	-	0.23	0.06	-
[NeV] 14.32	-	0.05	0.26	2.86	3.2	2.9	-	0.57	0.08	-
[NeV] 24.3	-	0.05	0.2	2.7	3.23	2.8	-	0.69	0.03	-
[SiVI] 1.96	-	3(-3)	1(-3)	0.33	0.34	0.07	-	0.55	0.17	-
[NeVI] 7.6	-	1(-3)	0.01	2.5	3.7	5.3	-	2.11	0.35	-
[FeVII] 6087	-	2.4(-3)	1(-3)	0.8	0.87	0.27	-	3.8	1.5	-
[SiVII] 2.48	-	-	-	0.2	0.35	0.26	-	0.86	1.3	-
[MgVII] 5.5	-	-	-	0.24	0.6	0.9	-	1.02	0.45	-
[SVIII] 9913	-	-	- ³⁵	0.1	0.2	0.4	-	0.17	0.9	-
[MgVIII] 3.03	-	-	-	0.08	0.28	0.95	-	0.8	1.35	-
[SIX] 1.25	-	-	-	.016	0.04	0.15	-	0.05	0.88	-
[SiIX] 2.59	-	-	-	0.13	0.5	2.23	-	0.46	8.4	-
[SiIX] 3.9	-	-	-	0.3	1.0	4.7	-	0.86	15.5	-
[FeX] 6374	-	-	-	0.12	0.27	0.67	-	0.83	12.7	-
[FeXI] 7892	-	-	-	0.04	0.13	0.5	-	0.09	0.04	-

Table 3 a
The optical and near-IR spectrum

line	obs/[O III]	MA	MB	MC	MD
HeII 4686	0.025	0.026	0.024	0.02	0.02
[OIII] 4959	0.3	0.3	0.3	0.3	0.3
[O III] 5007	1.	1.	1.	1.	1.
[NI] 5200	0.029	0.01	0.01	0.01	0.01
[FeVII] 6087	5.(-3)	5.4(-3)	0.01	9.(-3)	6.(-3)
[OI] 6300+	0.04	0.1	0.08	0.06	0.16
[FeX] 6374	7.7(-3)	7.(-3)	8.(-3)	5.2(-3)	4.(-3)
[NII] 6548+	0.36	0.33	0.24	0.30	0.46
[SII] 6716	0.07	0.1	0.08	0.07	0.07
[SII] 6730	0.07	0.1	0.09	0.077	0.09
[OII] 7320+	5.9(-3)	0.01	0.01	0.01	0.03
[FeXI] 7892	5.9(-3)	5.(-3)	5.4(-3)	3.1(-3)	3.(-3)
[SIII] 9069+	0.10	0.20	0.15	0.20	0.26
[CI] 9850	1.6(-3)	1.(-3)	5.(-4)	1.(-3)	0.02
[SVIII] 9913	3.7(-3)	4.(-3)	5.(-3)	3.3(-3)	3.(-3)
[SIX] 1.25	3.4(-3)	4.6(-3)	4.(-3)	3.0(-3)	1.(-3)
[SiVI] 1.96 ¹	6.(-3)	3.(-3)	5.4(-3)	3.(-3)	3.(-3)
[SiVII] 2.48	0.01	3.(-3)	6.1(-3)	4.(-3)	3.(-3)
[SiIX] 3.9	0.02	0.046	0.047	0.03	0.02

Line ratios are from Oliva et al. (1994) and are corrected by $A_v \sim 5.8$ mag. We assume 10% uncertainty for the stronger lines, 30% for weak and IR lines. Optical lines are from the central $1.5 \times 4.5 \text{ arcsec}^2$ region, IR lines from the central $4.4 \times 6.6 \text{ arcsec}^2$, thus only the IR coronal lines are modelled. ¹ Flux measured within the 15 pc region by (Maiolino et al. (1998) with 10% quoted error. The value measured in a 90×40 pc region by Oliva et al. differs by 15%.

Table 3 b
The IR spectrum

line	obs/[O IV]	MA	MB	MC	MD
[SiIX] 2.59 ¹	0.03	0.13	0.13	0.07	0.04
[MgVIII] 3.03	0.09	0.07	0.06	0.03	0.03
[SiIX] 3.9	0.07	0.33	0.3	0.14	0.1
[MgVII] 5.5	0.1	0.07	0.08	0.04	0.03
[MgV] 5.6 ¹	0.06	0.01	0.03	0.02	0.01
[NeVI] 7.6	0.6	0.41	0.5	0.30	0.20
[ArIII] 8.99	0.10	0.13	0.08	0.16	0.2
[SIV] 10.54	0.15	0.15	0.12	0.12	0.13
[[NeII] 12.8	1.1	0.04	0.02	0.06	0.52
[NeV] 14.32	0.6	0.33	0.4	0.23	0.2
[NeIII] 15.55	0.6	1.0	0.7	0.9	1.0
[SIII] 18.7	0.4	0.4	0.23	0.32	0.39
[NeV] 24.3	0.3	0.3	0.4	0.30	0.2
[OIV] 25.9	1.	1.	1.	1.	1.
[FeII] 26	0.11	0.3	0.2	0.23	0.4
[SIII] 33.5	1.9	0.5	0.4	0.40	0.43
[SiII] 34.86	2.2	0.8	0.5	0.70	0.9

ISO lines have errors of 30%. ¹ Weak lines in the spectrum.

Fig. 1 a

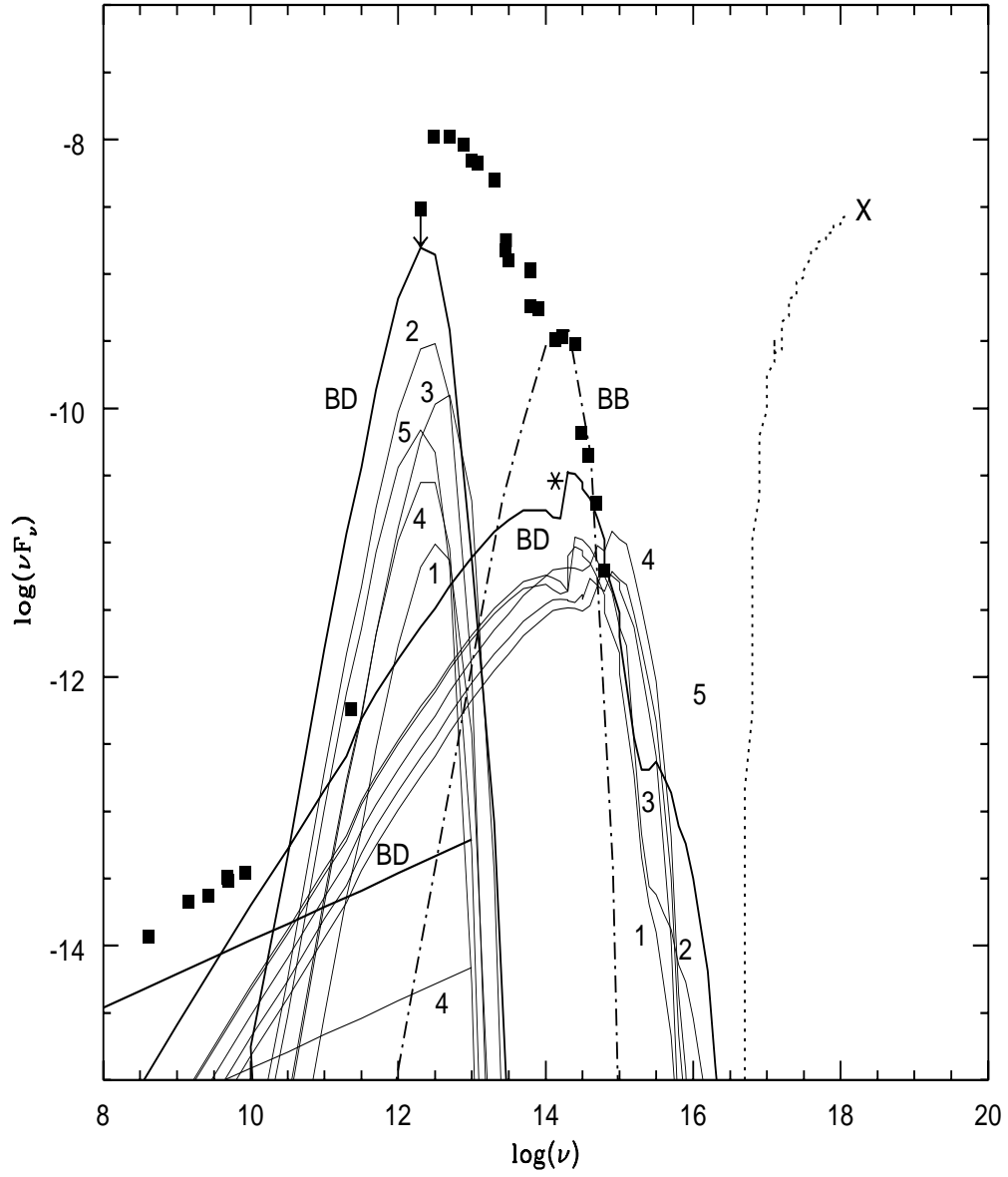


Fig. 1 b

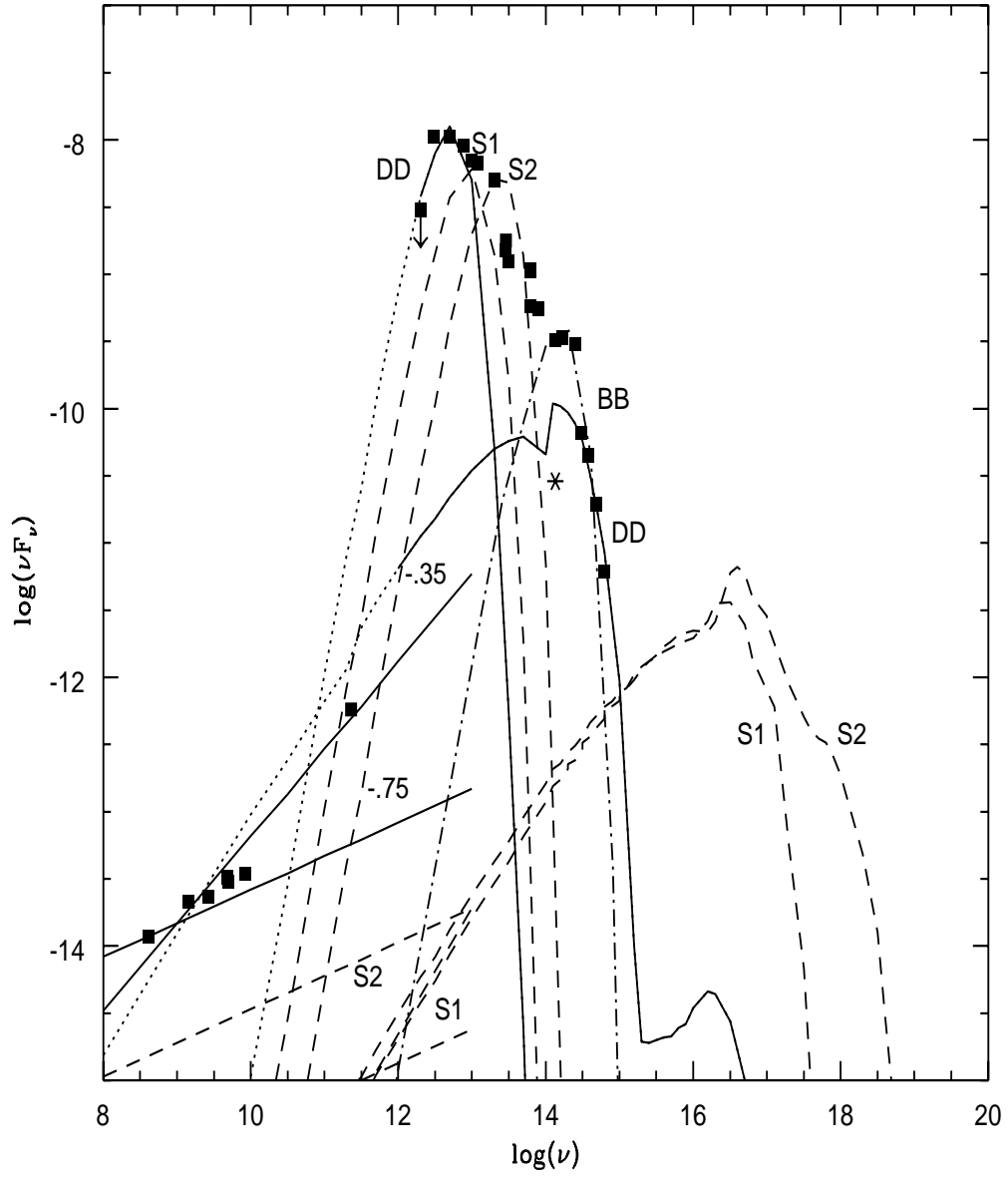


Fig. 2 a Fig. 2 b

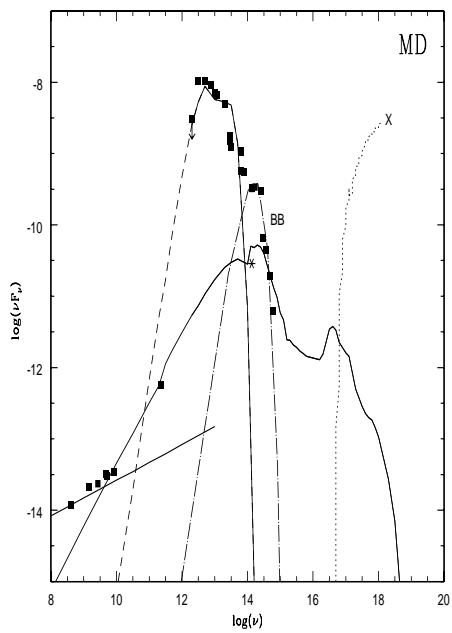
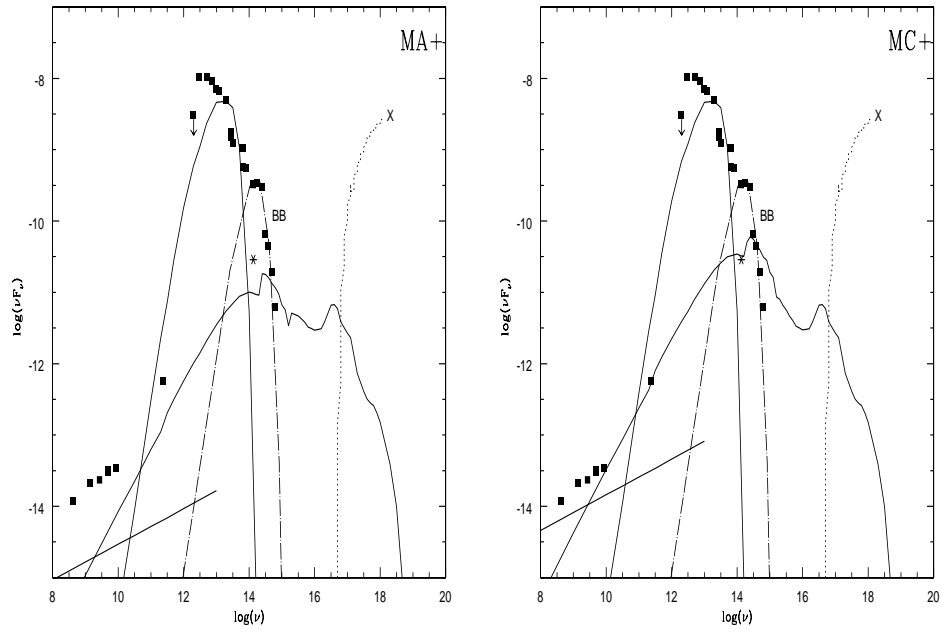


Fig. 2 c

Fig. 3 a

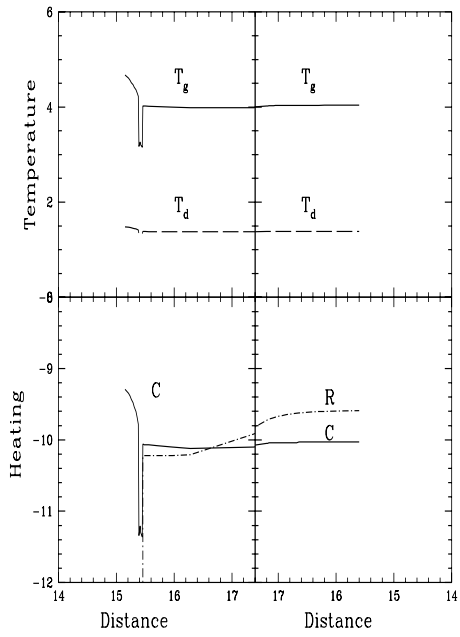


Fig. 3 b

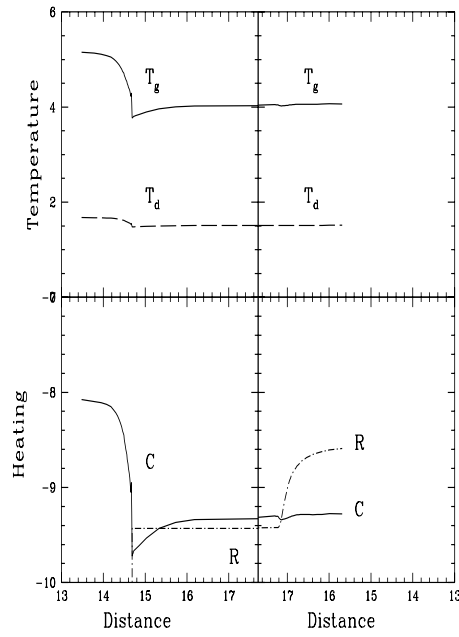


Fig. 3 c

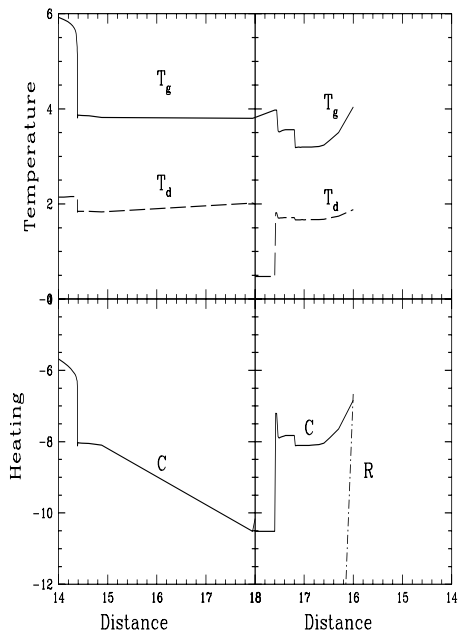


Fig. 3 d

